Monitoring the Lifetime of Photoexcited Electrons in a Fresh and Bulk Reduced Rutile TiO_2 Single Crystal. Possible Anisotropic Propagation

M. Alamoudi, K. Katsiev, and H. Idriss*

ABSTRACT: Defects (oxygen vacancies and interstitial cations) in oxide semiconductors have recently been invoked as a key property behind increased photocatalytic reaction rates. In this work, we have monitored by transient absorption spectroscopy (TAS) excited electrons in the conduction band decaying into the invoked traps to extract their lifetime using a rutile single crystal instead of the more conveniently used powder homologue. This is preferred in order to rule out grain boundary, degree of crystallinity, and size effects among other parameters that would obscure the results. It was found, in the energy region investigated (1.3−1.8 eV), that the lifetime of excited electrons is about four times shorter for the bulk defect crystal when compared to the fresh one. This indicates that the created defects (mostly oxygen defects and interstitial Ti cations) are unlikely to contribute to reaction rate enhancement.

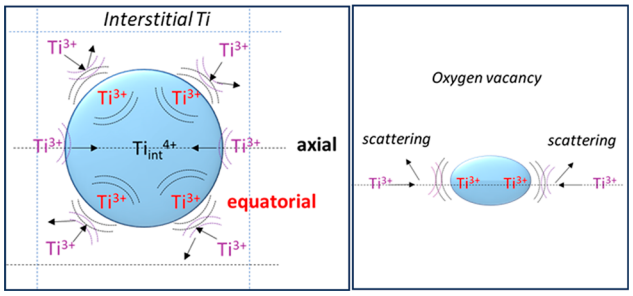

One of the main properties affecting the response of an oxide semiconductor to light is the presence of defects (such as oxygen defects and interstitial metal cations).[1] In recent years, there has been considerable interest in making defects in semiconductors to increase their photocatalytic (and in some cases the photoelectrocatalytic[2]) activity for hydrogen ions[3] and CO_2 reductions.[4] This is an intriguing approach. While defects, by introducing energy states within the forbidden energy gap, increase light absorption, the creation of defects in general decreases the quality of a semiconductor and therefore would be detrimental to charge propagation. In this work, we focus on the most common and studied two types of intrinsic defects in an n-type oxide semiconductor (oxygen defects and interstitial metal cations). The created oxygen defects may result in polaron formation when the left electrons interact with lattice phonons causing a structural distortion.[5] Similarly, the presence of interstitial cations results in lattice distortion which in turn leads to polaron formation.[6] There are also photoexcited polarons whereby excited electrons (from the valence band to the conduction band) interact with the lattice and propagate, temporally, in the semiconductor photocatalyst.[7] Therefore, there is an interplay between these three quasi-particles: two of them are in the ground state (polarons due to oxygen defects and interstitial cations) and one is in the excited state (the excited electron in the conduction band). The most studied and probably most understood metal oxide semiconductor with respect to thermal or photoexcited reactions is TiO_2 and in particular its rutile phase. This is because synthetic pure rutile single crystals are available and can be studied by multiple electronic[8,9] and diffraction[10,11] techniques.

Time resolved spectroscopy, at the femto- and picosecond scales, has been used for a few decades now to study excited charge carriers and charge transfer of materials.[12] It was initially developed to study molecules[13] and then extended to colloidal systems[14] (nanoparticles) and polycrystalline[15] materials. Information can be obtained related to interfacial charge transfer between semiconductors and between semiconductors and metals.[16] In general, there are three regions of investigation (neglecting the bleach state near the excitation energy): the energetically shallow region at a fraction of an eV from the CB (in the mid-IR region),[17] often attributed to excited polarons,[18] the near IR region[19] with an energy in the 1 to 2 eV range, mostly related to surface and bulk defects, and a visible region, mostly attributed to holes;[20,21] in wide band gap semiconductors it is above 2 eV.

While for molecular studies and largely for free nanoparticles, information may be directly transferred to more complex systems, working on polycrystalline materials has fewer general implications. This is because charge propagation in oxide semiconductors is sensitive to an overwhelmingly large

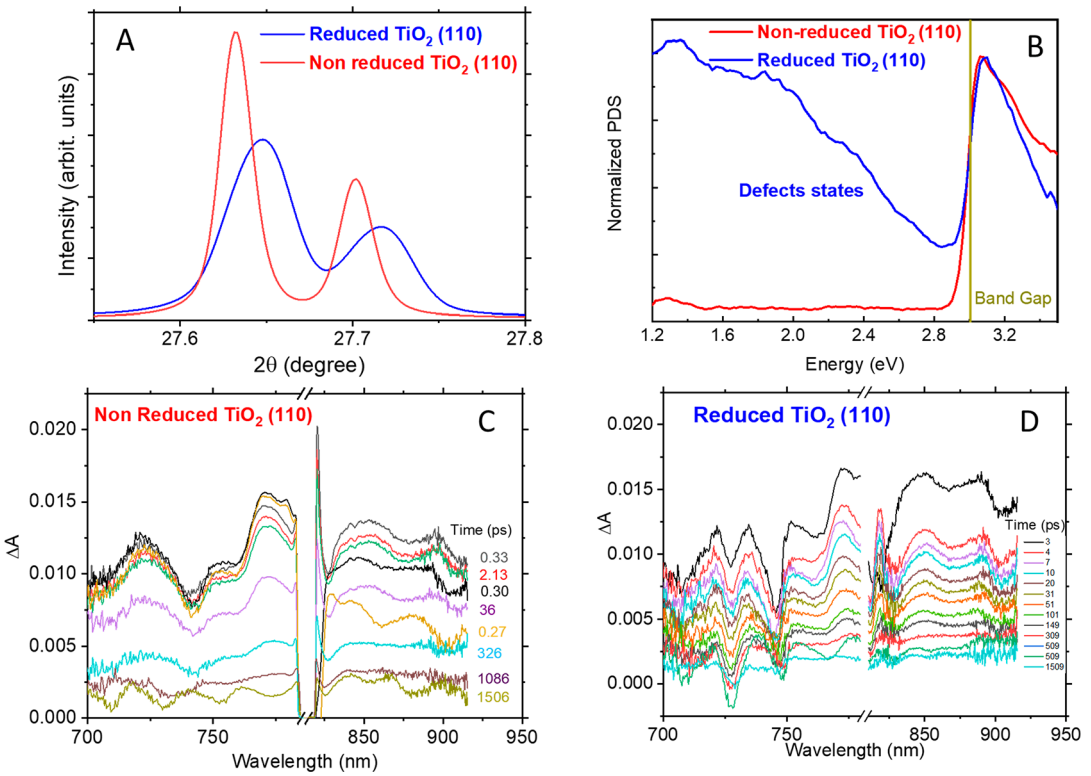

Figure 1. A. X-ray diffraction pattern of a fresh TiO_2(110) and after reducing it by heating in UHV for 60 min at ca. 850 K. B. Photothermal deflection spectroscopy (PDS) of a fresh TiO_2(110) and after reducing it by heating in UHV for 60 min at ca. 850 K. C. TAS signal decay of a fresh TiO_2(110) rutile single crystal. D. TAS signal decay of a bulk reduced TiO_2(110) rutile single crystal.

number of factors: their degree of crystallinity, polymorphs, crystallite size, lattice size that changes (expansion and contraction) with crystallite size, deviation from stoichiometry associated with the presence of surface and bulk defects, and grain boundaries, among many others. Therefore, extracting relevant information for a wider use such as to make a photocatalyst from first-principles is difficult if not impossible. Single crystals, however, while not perfect, offer a simpler method for investigation and have shown over the years a much higher degree of reproducibility of the results. This is because of the absence of grain boundaries, the negligible surface to bulk ratio, and the highest degree of crystallinity; all are poised to affect charge carrier lifetime.

Considerable effort on the study of the role of defects in oxides[22] and their proposed involvement in photo- and electrocatalytic reactions has been pursued. It is worth pointing out that in thermally driven catalytic reactions, surface oxygen defects indeed participate in the reaction, such as in the water gas shift reaction[23] and hydrocarbon oxidation.[24] In a photocatalytic system, their positive role on reaction rates is questionable. First, because the reaction occurs at low temperature (typically room temperature) which is too low for ionic movements needed to regenerate consumed defects in the first catalytic cycle.[25] Second, it is at odds with the requirement that charges propagate best in a perfect medium (nondefective); otherwise, their interaction with these charged defects would scatter them and therefore decrease their mobility and increase the probability of recombination with valence band holes.[26] It is therefore fundamentally not clear what is the role of these defects in a catalytic reaction of a photo excited system.

In this work, we have studied by time-resolved spectroscopy the lifetime of excited charges of about 1.35−1.8 eV on a stoichiometric (near perfect) TiO_2(110) rutile crystal and when bulk reduced by thermal heating. It was found that the creation of bulk defects in the rutile single crystal results in decreasing their lifetime. We then, based on these results, construct a scheme, albeit phenomenologically, on excited charge propagation in the rutile semiconductor.

METHODS

Transient absorption (TA) measurements were performed on 0.1 ps to 3 ns time scales which is based on a regeneratively amplified Ti:sapphire laser system (produces 800 nm laser pulses of 90 fs pulse width at a 1 kHz repetition rate) and in conjunction with Excipro pump−probe spectrometers (CDP, Moscow). The pump pulses at 305 nm were generated after passing through a fraction of an 800 nm beam into the spectrally tunable (240−2600 nm) optical parametric amplifier (TOPAS Prime, Spectra-Physics) and a frequency mixer (NIR Vis UV, Light conversion). The fluence of the pump power was adjusted by using neutral density (ND) filters to avoid multiple exciton generation (it was about 15 mW/cm^2). To generate the probe pulses (UV visible and NIR wavelength continuum), 10% of the 800 nm amplified pulses was focused onto the 2 mm thick calcium fluoride (CaF_2) crystal. To detect the transient species following excitation at different time scales, the 800 nm amplified pulses were passed through a motorized delay stage before the white light generation. To achieve better signal-to-noise ratios, the resulting white light was split into two channels (probe and reference) and focused on two fiber optics. The pump pulses (305 nm; above the BG of TiO_2) were overlapped on the TiO_2(110) single crystal and

Table 1. Fitting Parameters of the Biexponential Function for the Fresh and Reduced Rutile TiO_2(110) Single Crystal Together with the Computed Mean Life Time of the Signal

	N_1	τ_1 (ps)	N_2	τ_2 (ps)	$\langle t \rangle$ (s)	$\langle k \rangle$ (s^{-1})
			Stoichiometric TiO_2(110)			
770 nm (1.61 eV)	0.41	19.9	0.44	463	4.5×10^{-10}	
850 nm (1.46 eV)	0.34	19.2	0.40	362	3.5×10^{-10}	
					4×10^{-10}	**2.5×10^{9}**
			Reduced TiO_2(110)			
770 nm (1.61 eV)	0.47	4.6	0.48	95	0.9×10^{-10}	
850 nm (1.46 eV)	0.38	5.5	0.43	121	1.1×10^{-10}	
					1.0×10^{-10}	**1×10^{10}**

then reflected with a mirror to the detector, with the probe pulses after passing through a synchronized chopper (500 Hz) which blocked alternative pump pulses (Figure S1). Measurements were conducted at ambient conditions. The change in absorption (ΔA) of the excited state is calculated by subtracting absorption of the excited and unexcited samples.

Photothermal deflection spectroscopy (PDS) measurements were performed using a built-on purpose PDS setup. Light from a 250 W quartz-tungsten-halogen lamp (Newport 66996-250Q-R1) was sent through a monochromator (LOT MSH-300) and used as a pump, allowing excitation across the UV to NIR spectral region. The pump light was modulated by a chopper operating at a constant frequency of a few Hertz and focused on the TiO_2 single crystal. The single crystal was immersed in Perfluorohexane C_6F_{14} (Sigma-Aldrich) as a chemically inert liquid during the measurement. A small fraction of the monochromatic pump light was split off as intensity reference and measured by a lock-in detection (Stanford Research Systems SR830 4 lock-in amplifier) using a pyroelectric detector (Newport DET-L-PYC5-R-P). A stabilized cw-laser (Thorlabs HR S015 HeNe 633 nm) was used as probe beam source focused closely on the TiO_2 single crystal surface. The deviation of the probe beam was detected by a silicon quadrant detector (Thorlabs PDP90A) using lock-in detection (Stanford Research Systems SR830). The entire setup was controlled by LabView-based data acquisition and a device control code. The PDS spectra were set to the absolute scale by matching the spectra with integrating sphere measurements on a Varian Cary 6000 spectrophotometer.

The rutile (110) single crystal ($10 \times 10 \times 1$ mm^3) was purchased from MTI. The fresh sample was used as is after cleaning with ethanol in an ultrasound bath and then dried in ambient conditions. After the pump probe measurement was collected (in reflection mode, Figure S1), the same sample was mounted onto a Ta sample plate inside a UHV chamber and heated to 850 K for 1 h using an electron beam heating system. The temperature of the sample was monitored using a Sirius pyrometer by Process Sensors and a calibrated K-type thermocouple. XPS was performed in the same UHV system with a base pressure of 3×10^{-10} mbar equipped with a SPECS XR50 dual anode X-ray source (Al K_α was utilized) and a SCIENTA R3000 hemispherical electrostatic energy analyzer. XRD patterns were recorded by using a Bruker D8 Advance X-ray diffractometer. A 2θ interval between 20 and 90° was used with a step size of 0.010° and a step time of 0.2 s/step.

Figure 1A presents the diffraction pattern of a fresh TiO_2(110) single crystal before and after reduction with heating in UHV for 60 min at ca. 850 K. The two peaks for each sample are due to Cu K_α and Cu K_β of the X-ray source. Two main differences are seen upon bulk reduction: an increase in the peak width (fwhm) and a slight lattice contraction. The creation of defects decreased the crystallite domains from 280 to 150 nm, and the $d_{(110)}$ spacing was contracted by 0.03%. Contraction and expansion are anisotropic in rutile TiO_2; in general, very small changes have been reported for the different planes upon reduction.[27−29] XPS Ti 2p showed the expected presence of Ti^{3+} at ca. 457.5 eV upon reduction (not shown). The surface chemical state is not relevant for this study because measurements are conducted in ambient conditions, and therefore, the surface state is instantly oxidized, lattice oxygen diffusion is negligible at the time scale of the experiment, and because the signal contribution of the surface can be neglected for TAS measurements conducted on a single crystal (information typically is obtained from about 200 layers using an excitation light with a 305 nm wavelength).

Figure 1B presents PDS of the fresh and reduced TiO_2(110) single crystal. The band gap of the rutile phase is at ca. 3.0 eV, and the absorption above this energy is clear. This is analogous to UV−vis measurements routinely conducted for powder[30,31] for both stoichiometric and reduced TiO_2. In PDS however, it is the nonradiative decay that produces heat that changes the reflective index which is turn is monitored by a probe light[32,33] (see Methods). The crystal in both states largely absorbs above 3.0 eV. However, the reduced surface shows considerable absorption below the band gap energy due to the creation of defects upon annealing to high temperatures in vacuum. It is to be noted that these are bulk defects because surface defects would be instantaneously healed by O_2 and water molecules of the ambient environment during TAS collection. Therefore, the TAS results would originate from bulk defects.

Figures 1C and 1D present TAS of the fresh and bulk reduced TiO_2(110) in the region 700−920 nm (1.35−1.8 eV). The shape of the signal is determined by many factors including the white light (probe), the excitation energy, the lattice structure, and temperature. This has been studied in great detail on colloidal systems from which one may gather some information. In short it was found, by changing the size of a given semiconductor, that the absorption cross section is α to R (the size) at low energy and α to R^3 at high energy.[34] One may then infer that a crystal with a high concentration of reduced states (energy states), Figure 1C, has more overall overlap with optical transition than another one with much less defects. The transient signal increases very fast, within 1 ps, and then decays thereafter. The signal decay in this region was analyzed and fitted to compare both fresh and reduced crystals. The signal is fitted by a biexponential decay, and the results are given in Table 1. While a triexponential decay was in some cases a better fit (see below), it was opted to keep the biexponential fitting to simplify the analysis. Figure 2 presents

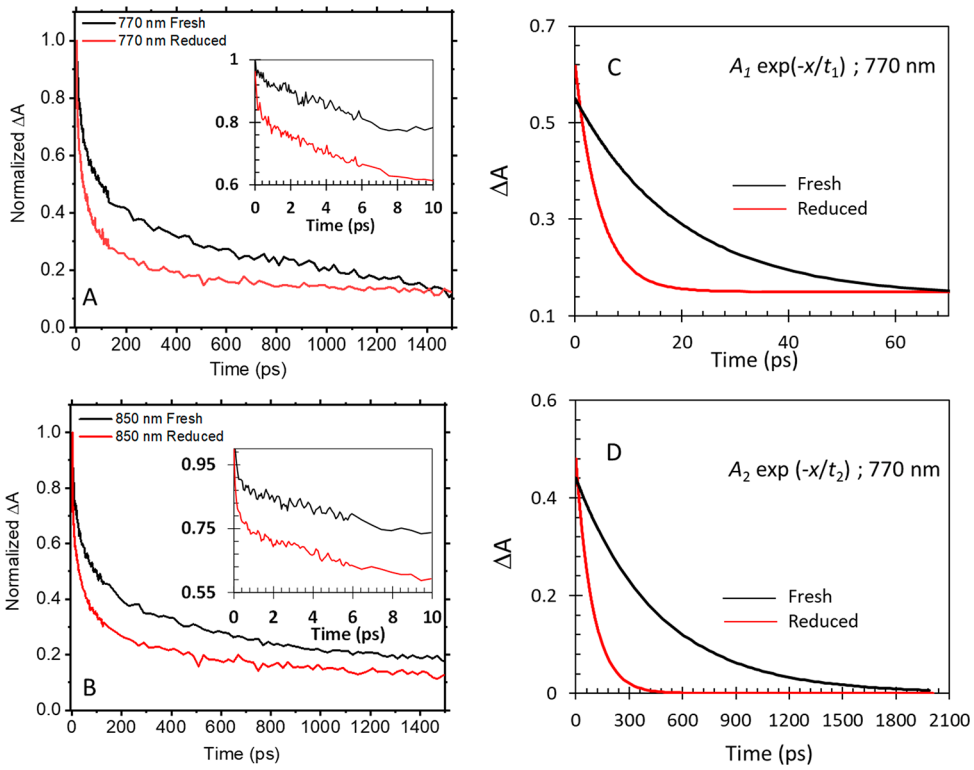

Figure 2. A. and B. Kinetic traces of the transient signal in the near IR of the fresh and reduced TiO_2(110) single crystals at 770 and 850 nm. C. and D. First and second components of the exponential decay for the signal at 770 nm.

Scheme 1. A. 2-D Representation (*xz*) of Stoichiometric Rutile TiO_2 along the [001] Direction (*x*-Axis). B. The Same as A, upon the Removal of an Oxygen Atom. C. Excited Electrons upon Pulse Excitation Propagating along the [001] Direction Represented by Ti^{3+} Cations in Pink. D. The Same as in C, in the Presence of the Two Electrons Left in the Lattice upon the Removal of an Oxygen Atom.[a] E. An Interstitial Ti Cation Surrounded by Four Equatorial and Two Axial Ti Cations[b]. F. A Similar Plot to D, to Highlight the Size Difference between Ti^{3+} Cation Centers Formed Due to the Removal of One Oxygen Atom with That Much Larger, Formed upon the Formation of an Interstitial Ti^{4+} Cation in E

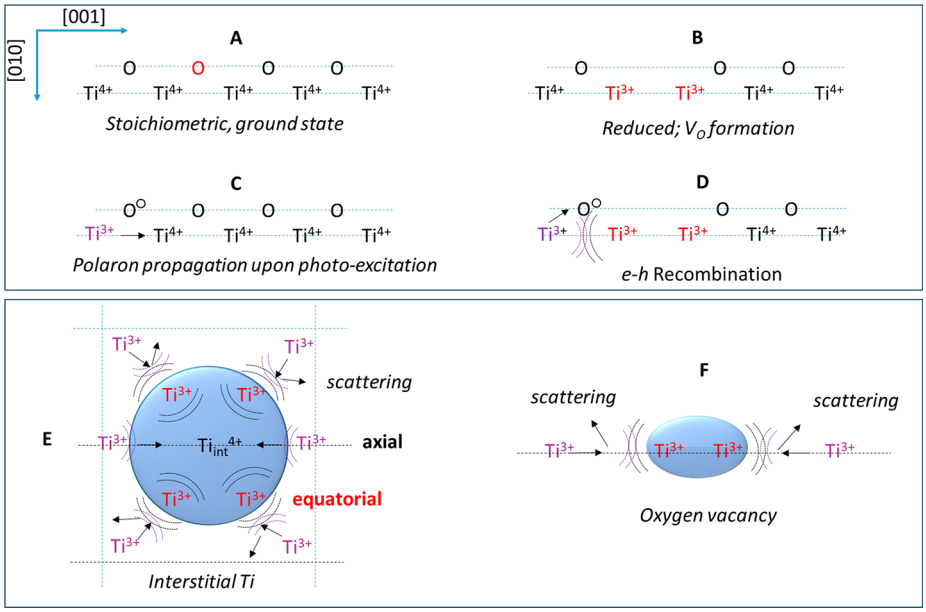

[a]The semicircles around the Ti^{3+} cations represent the electron density due to the $3d^1$ electrons on each Ti cation. Note that the Ti^{3+} cations in red are in ground state polarons, while those in pink are for excited state polarons. [b]The four equatorial Ti cations are in the +3 oxidation state considering that the interstitial Ti metal has given away its four electrons and therefore ground state polarons. The two equatorial Ti cations are in the +3 oxidation state due to photo-excited electrons. The other four Ti^{+3} cations are also photo-excited polarons.

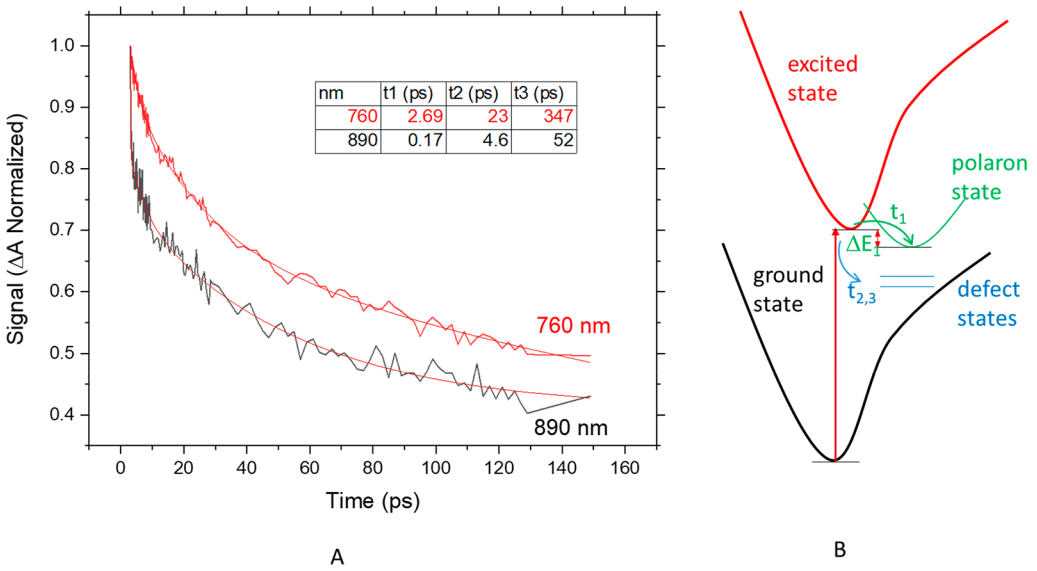

Figure 3. A. Comparison of the initial TAS signal decay at 760 and 890 nm for the fresh rutile TiO_2(110) single crystal. To highlight the decay, a triexponential decay function was used for the fit between 0 and 150 ps (R^2 = 0.983). B. A schematic of the decaying events of excited electrons from the valence band (ground state) to the conduction band (excited state) (direct band gap excitation). Defect states are those of interstitial Ti cations and O vacancies. Strictly, the polaronic state is much shallower in energy than the defect state. It is assumed that the signal at 890 nm still contains information from the high energy side of polaronic states.

the signal decay at two representative regions (770 and 850 nm). The signal decay is much faster on the bulk-reduced crystal. This decay affects both exponential parts of the fitting as seen in Figure 2C and D where the two components are plotted.

The two lifetimes for the signal decay (t_1 and t_2) decreased by a factor of about 4 for the reduced crystal when compared to the fresh one. The weighted average lifetime was found to be 4×10^{-10} s for the fresh crystal and 1×10^{-10} s for the reduced crystal, from which the rate constants 2.5×10^9 s^{-1} and 1×10^{10} s^{-1} were obtained, respectively. Because the origin of the decays is still a matter of interpretation, we address it in the following.

The disappearance of the signal indicates that excited electrons of this energy range lose their energy upon some type of interaction with the lattice, and this loss is not homogeneous as it is fitted by two time constants. TiO_2 has Ti^{3+} in the lattice as defects (due to the removal of oxygen atoms) as well as interstitial Ti cations (mostly Ti^{3+} cations); the Magneli phase is one of them.[35] These two types of defects have been studied computationally, among other methods, on rutile TiO_2. While both falls at about 1 to 2 eV below the conduction band, the energy of the interstitial Ti defect is closer to the conduction band (by about 0.2 eV) than that of oxygen vacancies.[36] Moreover, their relative concentration changes with the preparation conditions. Annealing to high temperatures in the absence of molecular oxygen, as under UHV conditions, favors the formation of interstitial centers. It is not clear what these ground state defects do to the photoexcited electrons. To help visualize this, the following scheme is drawn.

We start from the point that defects in an n-type oxide semiconductor are negatively charged. Therefore, a photo-excited electron decaying from the conduction band is repulsed by these defects. In other words, strictly they are not trapped, at least not in these centers. The charge disappears upon losing its energy, facilitated by the repulsion from these centers. This is the proposed concept in Scheme 1. In the scheme, the oxygen vacancy is not drawn, upon the removal of a lattice oxygen atom; the only matter left is the two electrons transferred to two Ti^{4+} cations that become Ti^{3+} cations. For simplicity, they are drawn next to each other,[37] but they do not need to be.[38] In Scheme 1C, an excited charge propagates along one direction (for simplicity). These have been studied by others and are at the origin of IR interrogated signals.[39,40] Charge propagation has low activation energy[41] allowing it to occur at room temperature and below. Scheme 1D shows the effect of the removal of a bulk oxygen atom on the propagation. The presence of Ti^{3+} cations would result in scattering of the excited electron which may then need to cross a higher barrier than along the [001] (the Ti−Ti distance of ca. 3 A which is the shortest), and this would result in slowing its propagation. Slowing the propagation may be viewed as a trap, because an activation barrier needs to be crossed, yet it may also result in increased recombination with holes on the adjacent oxygen atoms. The activation energies of anisotropic charge propagation in oxides have been computed and show that it can vary significantly.[42−45] Scheme 1E presents charge propagation close to an interstitial Ti cation. The charge of an interstitial Ti ($Ti_{int.}$) cation can vary. Starting from $Ti_{int.}$, the most stable ground state configurations were found to be that of $Ti_{int.}^{3+}$ (surrounded by three Ti^{3+} cations) and $Ti_{int.}^{4+}$ (surrounded by four Ti^{3+} cations). Taking $Ti_{int.}^{4+}$ as an example, charge propagation would occur through one of the four equatorial adjacent Ti^{3+} cations or through one of the two axial Ti^{4+} cations. In this configuration, charge will preferentially propagate along the axial Ti^{4+} cations toward the $Ti_{int.}^{4+}$ cations. This is because they will be less scattered. If this occurs, it is possible that the charge is trapped, aided by the repulsion from the four equatorial Ti^{3+} cations until it reacts with a hole residing on one of the surrounding lattice oxygen anions.

Closer inspection of the signal decay in the monitored area showed some inhomogeneity with the decay with wavelengths. The high-energy side (at about 1.7 eV) decays slower than the

low energy side (at about 1.4 eV) in a very short time. This is particularly noticeable for the fresh sample, although the bulk-reduced surface still showed the same trend (Figure S2). This is presented in Figure 3 where the very sharp decay with time at 890 nm is clear for the fresh sample. Figure S3 shows the trend of a more complete region. These decays most likely translate the different types of centers that interact with the photoexcited electrons. The very fast decay at the low energy side can be computed by fitting a triexponential decay function, from which t_1 was found to decrease from 2.7 to 0.17 ps (within the time resolution limit of the spectrometer). This can be linked to small polarons of the excited state self-trapped conduction band electrons. A polaron's lifetime on a rutile TiO_2 single crystal has been experimentally[46] measured and found to be of the order of 50 fs and computed by others and found to be about 25 fs.[47]

Based on the above results, the simplest conclusion would be that bulk defects in rutile single crystals decrease the lifetime of excited electrons in the region traditionally assigned to trapped electrons around the O vacancies and interstitial Ti cations. When the decay is fitted by two time constants, it is found that both decrease four times when the domain size decreases by about two (from 280 to 150 nm). It is argued that the effect of defects is different on the decay. Oxygen defects would slow the propagation because electron hopping will need to change direction, while in the case of Ti_{int}, it is due to orienting the propagation preferentially along the axial Ti cations. Yet, increasing their number (oxygen defects and Ti interstitial) results in an overall decrease of the lifetime of excited electrons, irrespectively. The overall decrease of the lifetime of the charge propagation with bulk defects is not in favor of their proposed photocatalytic activity.

AUTHOR INFORMATION

Corresponding Author

H. **Idriss** − *Institute of Functional Interfaces, Karlsruhe Institute of Technology (KIT), 76344 Eggenstein-Leopoldshafen, Germany; Department of Chemistry, University College London, WC1H 0AH London, U.K.;* orcid.org/0000-0001-8614-7019; Email: Hicham.idriss@kit.edu, h.idriss@ucl.ac.uk

Authors

M. Alamoudi − *Surface Science and Advanced Characterization, SABIC-CRD at KAUST, Thuwal 23955, Saudi Arabia*

K. Katsiev − *Surface Science and Advanced Characterization, SABIC-CRD at KAUST, Thuwal 23955, Saudi Arabia*

Notes

The authors declare no competing financial interest.

ACKNOWLEDGMENTS

The authors thank Prof. Frédéric Laquai and his team at the KAUST Solar Center for providing the PDS facility to M. Alamoudi to conduct the measurements.

REFERENCES

(1) Kim, K.; Yu, J.; Noh, J.; Reimnitz, L. C.; Chang, M.; Gamelin, D. R.; Korgel, B. A.; Hwang, G. S.; Milliron, D. J. Synthetic Control of Intrinsic Defect Formationin Metal Oxide Nanocrystals Using Dissociated Spectator Metal Salts. *J. Am. Chem. Soc.* **2022**, *144* (50), 22941−22949.

(2) Balog, Á.; Samu, G. F.; Pető, S.; Janáky, C. The Mystery of Black TiO_2: Insights from Combined Surface Science and In Situ Electrochemical Methods. *ACS Mater. Au* **2021**, *1*, 157−168.

(3) Chen, X.; Liu, L.; Yu, P. Y.; Mao, S. S. Increasing Solar Absorption for Photocatalysis with Black Hydrogenated Titanium Dioxide Nanocrystals. *Science* **2011**, *331*, 746−750.

(4) Piler, K.; Bahrim, C.; Twagirayezu, S.; Benson, T. J. Lattice Disorders of TiO_2 and Their Significance in the Photocatalytic Conversion of CO_2. *Adv. Catal.* **2020**, *66*, 109−233.

(5) Bandaranayake, S.; Hruska, E.; Londo, S.; Biswas, S.; Baker, R. Small Polarons and Surface Defects in Metal Oxide Photocatalysts Studied Using XUV Reflection−Absorption Spectroscopy. *J. Phys. Chem. C* **2020**, *124*, 22853−22870.

(6) Finazzi, E.; Di Valentin, C.; Pacchioni, G. Nature of Ti Interstitials in Reduced Bulk Anatase and Rutile TiO_2. *J. Phys. Chem. C* **2009**, *113*, 3382−3385.

(7) Gao, C.; Zhang, L.; Zheng, Q.; Zhao, J. Tuning the Lifetime of Photoexcited Small Polarons on Rutile TiO_2 Surface via Molecular Adsorption. *J. Phys. Chem. C* **2021**, *125*, 27275−27282.

(8) Jones, R.; D'Acunto, G.; Shayesteh, P.; Rehman, F.; Schnadt, J. AP-XPS Study of Ethanol Adsorption on Rutile TiO_2(110). *J. Phys. Chem. C* **2022**, *126* (39), 16894−16902.

(9) Dong, S.; Xia, S.; Wang, C.; Dong, J.; Wang, T.; Li, R.; Ren, Z.; Dai, D.; Yang, X.; Zhou, C. Valence Band of Rutile TiO_2(110) Investigated by Polarized-Light-Based Angle-Resolved Photoelectron Spectroscopy. *J. Phys. Chem. Lett.* **2022**, *13* (10), 2299−2305.

(10) Shirasawa, T.; Voegeli, W.; Arakawa, E.; Takahashi, T.; Matsushita, T. Structural Change of the Rutile−TiO_2(110) Surface During the Photoinduced Wettability Conversion. *J. Phys. Chem. C* **2016**, *120*, 29107−29115.

(11) Treacy, J. P. W.; Hussain, H.; Torrelles, X.; Cabailh, G.; Bikondoa, O.; Nicklin, C.; Thornton, G.; Lindsay, R. Structure of a Superhydrophilic Surface: Wet Chemically Prepared Rutile-TiO_2(110)(1 × 1). *J. Phys. Chem. C* **2019**, *123* (13), 8463−8468.

(12) Geiregat, P.; Carmelita Rodá, C.; Tanghe, I.; Singh, S.; Di Giacomo, A.; Lebrun, D.; Grimaldi, G.; Jorick Maes, J.; Van Thourhout, D.; Moreels, I.; Houtepen, A. J.; Zeger Hens, Z. Localization-Limited Exciton Oscillator Strength in Colloidal CdSe Nanoplatelets Revealed by the Optically Induced Stark Effect. *Light: Science & Applications* **2021**, *10* (1−11), 112.

(13) Moya, R.; Kondo, T.; Norris, A. C.; Schlau-Cohen, A. S. Spectrally-Tunable /Femtosecond Single-Molecule Pump-Probe Spectroscopy. *Opt. Express* **2021**, *29*, 28246.

(14) Ishibashi, Y.; Kawasaki, R.; Kihara, R.; Kawai, T.; Asah, T. Femtosecond Pump-Probe, Single-Particle Spectroscopic Study on Excited-State Migration Dynamics of Copper Hexadecafluorophthalocyanine Nanorods. *J. Phys. Chem. C* **2021**, *125* (49), 27260−27266.

(15) Wang, J.; Naixing Feng, N.; Sun, Y.; Mu, X. Nanoplasmon−Semiconductor Hybrid for Interface Catalysis. *Catalysts* **2018**, *8* (10), 429.

(16) Isimjan, T. T.; Maity, P.; Ahmed, T.; Mohammed, O. F.; Idriss, H. Relationship between the Photocatalytic Hydrogen Ion Reduction and Charge Carrier Dynamics of Pt/$Cd_{1-x}Ni_xS$ Catalysts. *J. Phys. Chem. C* **2019**, *123*, 24051−24061.

(17) Yamakata, A.; Vequizo, J. J. M.; Matsunaga, H. Distinctive Behavior of Photogenerated Electrons and Holes in Anatase and Rutile TiO_2 Powders. *J. Phys. Chem. C* **2015**, *119*, 24538−24545.

(18) Savory, D. M.; McQuillan, A. J. IR Spectroscopic Behavior of Polaronic Trapped Electrons in TiO2 under Aqueous Photocatalytic Conditions. *J. Phys. Chem. C* **2014**, *118*, 13680−13692.
(19) Khan, M. A.; Maity, P.; Al-Oufi, M.; Al-Howaish, I. K.; Idriss, H. Electron Transfer of the Metal/Semiconductor System in Photocatalysis. *J. Phys. Chem. C* **2018**, *122*, 16779−16787.
(20) Chu, W.; Saidi, W. A.; Zheng, Q.; Xie, Y.; Zhenggang, L.; Prezhdo, O. V.; Hrvoje Petek, H.; Zhao, J. Ultrafast Dynamics of Photongenerated Holes at a CH_3OH/TiO_2 Rutile Interface. *J. Am. Chem. Soc.* **2016**, *138*, 13740−13749.
(21) Onda, K.; Li, B.; Zhao, J.; Jordan, K. D.; Yang, J.; Petek, H. Wet Electrons at the $H_2O/TiO_2(110)$ Surface. *Science* **2005**, *308*, 1154.
(22) Xie, C.; Yan, D.; Li, H.; Du, S.; Chen, W.; Wang, Y.; Zou, Y.; Ru Chen; Wang, S. Defect Chemistry in Heterogeneous Catalysis: Recognition, Understanding, and Utilization. *ACS Catal.* **2020**, *10*, 11082−11098.
(23) Vecchietti, J.; Bonivardi, A.; Xu, W.; Stacchiola, D.; Delgado, J. J.; Calatayud, M.; E Collins, S. E. Understanding the Role of Oxygen Vacancies in the Water Gas Shift Reaction on Ceria-Supported Platinum Catalysts. *ACS Catal.* **2014**, *4* (6), 2088−2096.
(24) Gambo, Y.; Adamu, S.; Abdulrasheed, A. A.; Lucky, R. A.; Ba-Shammakh, M. S.; Hossain, M. M. Catalyst Design and Tuning for Oxidative Dehydrogenation of Propane -A Review. *Appl. Catal. A Gen.* **2021**, *609* (1−23), 117914.
(25) Idriss, H. Oxygen Vacancies Role in Thermally Driven and Photon Driven Catalytic Reactions. *Chem. Catalysis* **2022**, *2*, 1549.
(26) Wang, H.; Zhang, C.; Rana, F. Ultrafast Dynamics of Defect-Assisted Electron−Hole Recombination in Monolayer MoS_2. *Nano Lett.* **2015**, *15* (1), 339−345.
(27) Kuznetsov, A. Y.; Machado, R.; Gomes, L. S.; Achete, C. A.; Swamy, V.; Muddle, B. C.; Prakapenka, V. Size Dependence of Rutile TiO_2 Lattice Parameters Determined via Simultaneous Size, Strain, and Shape Modeling. *Appl. Phys. Lett.* **2009**, *94* (1−3), 193117.
(28) Santara, B.; Giri, P. K.; Imakita, K.; Fujii, M. Microscopic Origin of Lattice Contraction and Expansion in Undoped Rutile TiO_2 Nanostructures. *Phys. D: Appl. Phys.* **2014**, *47* (1−13), 215302.
(29) Shin, J. Y.; Joo, J. H.; Samuelis, D.; Maier, J. Oxygen-Deficient $TiO_{2-\delta}$ Nanoparticles via Hydrogen Reduction for High Rate Capability Lithium Batteries. *Chem. Mater.* **2012**, *24*, 543−551.
(30) Saadallah, F.; Yacoubi, N.; Genty, F.; Alibert, C. Photothermal Investigations of Thermal and Optical Properties of GaAlAsSb and AlAsSb Thin Layers. *J. Appl. Phys.* **2003**, *94*, 5041−4048.
(31) Zusan, A.; Vandewal, K.; Allendorf, B.; Hansen, N. H.; Jens Pflaum, J.; Salleo, A.; Dyakonov, V.; Deibel, C. The Crucial Influence of Fullerene Phases on Photogeneration in Organic Bulk Heterojunction Solar Cells. *Adv. Energy Mater.* **2014**, *4* (1−7), 1400922.
(32) Liu, Y.; Tian, L.; Tan, X.; Xin Li, X.; Chen, X. Synthesis, Properties, and Applications of Black Titanium Dioxide Nanomaterials. *Sci. Bull.* **2017**, *62*, 431−441.
(33) Nadeem, M. A.; Al-Oufi, M.; Wahab, A. K.; Anjum, D.; Idriss, H. Hydrogen Production on Ag-Pd/TiO_2 Bimetallic Catalysts: Isthere a Combined Effect of Surface Plasmon Resonancewith Schottky Mechanism on the Photo-Catalytic Activitys? *Chemistry Select* **2017**, *2*, 2754−2762.
(34) Klimov, I. Optical Nonlinearities and Ultrafast Carrier Dynamics in Semiconductor Nanocrystals. *J. Phys. Chem. B* **2000**, *104*, 6112−6123.
(35) Zhang, Q.; Liu, W.; Zhou, Y.; Li, J.; Sun, T.; Liu, Q.; Ma, Y.; Wang, J.; Li, Jun; Zhao, R.; et al. Andersson-Magnéli Phases Ti_nO_{2n-1}: Recent Progress Inspired by Swedish Scientists. *Z. Anorg. Allg. Chem.* **2021**, *647*, 126−133.
(36) Morgan, B. J.; Graeme, W.; Watson, G. W. Intrinsic n-Type Defect Formation in TiO_2: A Comparison of Rutile and Anatase from GGA+U Calculations. *J. Phys. Chem. C* **2010**, *114*, 2321−2328.
(37) Morgan, B. J.; Watson, G. W. A Density Functional Theory + U Study of Oxygen Vacancy Formation at the (110), (100),(101), and (001) Surfaces of Rutile TiO_2. *J. Phys. Chem. C* **2009**, *113*, 7322−7328.
(38) Deskins, N. A.; Rousseau, R.; Dupuis, M. Distribution of Ti^{3+} Surface Sites in Reduced TiO_2. *J. Phys. Chem. C* **2011**, *115*, 7562−7572.
(39) Panayotov, D. A.; Burrows, S. P.; Morris, J. R. Infrared Spectroscopic Studies of Conduction Band and Trapped Electrons in UV-Photoexcited, H-Atom n-Doped, and Thermally Reduced TiO_2. *J. Phys. Chem. C* **2012**, *116*, 4535−4544.
(40) Fu, Z.; Onishi, H. Infrared and Near-Infrared Spectrometry of Anatase and Rutile Particles Bandgap Excited in Liquid. *J. Phys. Chem. B* **2023**, *127*, 321−327.
(41) Franchini, C.; Reticcioli, M.; Setvin, M.; Diebold, U. Polarons in materials. *Nature Rev. Mater.* **2021**, *6*, 560−586.
(42) Hollander, L. E., Jr.; Castro, P. L. Anisotropic Conduction in Nonstoichiometric Rutile (TiO_2). *Phys. Rev.* **1960**, *119*, 1882−1885.
(43) Byl, O.; Yates, J. T., Jr. Anisotropy in the Electrical Conductivity of Rutile TiO2 in the (110) Plane. *J. Phys. Chem. B* **2006**, *110*, 22966−22967.
(44) Solanki, V.; Joshi, S. R.; Mishra, I.; Kanjilal, D.; Varma, S. Formation of Anisotropic Nanostructures on Rutile $TiO_2(110)$ Surfaces and Their Photo-Absorption Properties. *Metallurgical & mater. Trans. A* **2018**, *49A*, 3117−3121.
(45) Williams, O. B. J.; Baek, B.; Harrison, G. T.; Katsiev, K.; Thornton, G.; Idriss, H. Direct Visualization of a Gold Nanoparticle Electron Trapping Effect. *J. Am. Chem. Soc.* **2022**, *144*, 1034−1044.
(46) Zhang, Y.; Payne, D. T.; Pang, C. L.; Cacho, C.; Chapman, R. T.; Springate, E.; Fielding, H. H.; Thornton, G. State-Selective Dynamics of TiO_2 Charge-Carrier Trapping and Recombination. *J. Phys. Chem. Lett.* **2019**, *10*, 5265−5270.
(47) Gao, C.; Zhang, L.; Zheng, Q.; Zhao, J. Tuning the Lifetime of Photoexcited Small Polarons on Rutile TiO_2 Surface via Molecular Adsorption. *J. Phys. Chem. C* **2021**, *125*, 27275−27282.